

Articles

https://doi.org/10.20884/1.jm.2025.20.3.14461

Band Gap Energy of Some Kekuléan Polycyclic Aromatic Hydrocarbon as Finite-Size Graphene: A DFT Study

Hafiz Aji Aziz^{1,2*}, Fadjar Mulya^{3*}, Thanawit Kuamit⁴, Harno Dwi Pranowo¹

¹Austrian-Indonesian Centre for Computational Chemistry, Department of Chemistry, Faculty of Mathematics and Natural Sciences, Universitas Gadjah Mada, Yogyakarta, 55281, Indonesia

²Department of Chemistry Education, Universitas Pendidikan Indonesia, Bandung 40154, Indonesia
³Nanotechnology Engineering Program, Faculty of Advanced Technology and Multidiscipline, Universitas
Airlangga, Surabaya 60115, Indonesia

⁴Center of Excellence in Computational Chemistry (CECC), Department of Chemistry, Faculty of Science, Chulalongkorn University, Pathumwan, Bangkok 10330, Thailand

*Corresponding author email: ha.aziz@upi.edu, fadjar.mulya@ftmm.unair.ac.id

Received February 07, 2025; Accepted October 06, 2025; Available online November 20, 2025

Abstract. The effect of size and shapes of some Kekuléan Polycyclic Aromatic Hydrocarbon (PAH) were studied using the density functional theory with B3LYP hybrid function and LANL2DZ basis set using Gaussian09 software program. Four different geometries of PAH: Linear (L), Hexagonal (H), Zigzag (Z) and Rhombus (R) were evaluated. The results showed that band gap energy (Eg) tends to decrease as the size of the increase, but some geometry decrease faster. Simple analysis also showed that $|\log(N)| = o(Eg(N))$ for L, H and R geometries, indicating that Eg will become 0 for a finite size. These trends indicate that PAH size and shape can be tuned to modulate electronic properties and redox behavior, offering routes to optimize PAH-based anodes for LIBs. In terms of industrial relevance, the ability to tailor Eg through geometry provides design guidelines to achieve higher energy density, faster charging, and improved cycling stability, while potentially enabling scalable and cost-effective synthesis and processing of carbon-based organic electrode materials. The findings support the development of PAH-based anodes as a viable pathway to enhance performance and manufacturability in lithium-ion battery technology.

Keywords: Density functional theory, electronic structure, energy materials, polycyclic aromatic hydrocarbons, shape effect, size effect.

INTRODUCTION

Graphene, an allotrope of carbon comprising atom-thick sheets arranged in a hexagonal pattern (Katsnelson, 2020; Muthuvinayagam, Ashok Kumar, Ramesh, & Ramesh, 2023; Saito, Dresselhaus, Dresselhaus, Dresselhaus, & Dresselhaus, 1998), exhibits intriguing mechanical, optical, and electronic properties (Naumis, Barraza-Lopez, Oliva-Leyva, & Terrones, 2017; Papageorgiou, Kinloch, & Young, 2017; Rozhkov, Sboychakov, Rakhmanov, & Nori, potential applications lts encompass metamaterial (Alden Mostaan & Saghaei, 2021; Jiang et al., 2021; Lin, Lin, Yang, & Jia, 2020; Qi et al., 2020), transistors (Fakih et al., 2020; Guo, Zhang, & Chan, 2021; Kim, Fan, Lee, Joo, & Lee, 2020; Wen, Yan, & Sun, 2020) and energy storage (Kumar et al., 2020; F. Mulya & Parasuk; A. Wang, Zhao, Yu, & Wang, 2021) Synthesis methods include mechanical exfoliation, a cost-effective technique with limitations such as micron-sized products, irregular shapes, and complexity. Alternatively, chemical vapor deposition (CVD) yields thin films of single or few-layer graphene, while microwave radiation synthesizes graphene materials from graphene-oxide precursors (Rahayu, Bunnari, & Hardyansyah, 2020).

Considering its planar hexagonal structure, graphene serves as an upper limit for polycyclic aromatic hydrocarbons (PAHs). The IUPAC formally defines graphene as a 'quasi-infinite PAH. Despite this relationship, the distinct sizes of PAHs and graphene result in significantly different properties. Previous studies, utilizing Extended Hückel Molecular Orbital methods, asserted that the energy gap (Eg) of hexagonal PAHs never reaches 0 eV, in contrast to experimental results (Tyutyulkov, Madjarova, Dietz, & Müllen, 1998). Additionally, these studies often neglected alternative geometries in their calculations, despite their potential applications.

In the realm of electronic applications, graphene and PAHs demonstrate significant promise. (Aumaitre & Morin, 2019) underscore the untapped potential of all-carbon PAHs specifically in organic electronics, highlighting their exceptional optical density, reversible redox processes, solubility, tunable band

gaps, and promising charge transport. Researchers are encouraged to explore these carbon-based materials for potential breakthroughs in the field of organic electronics. (Larik et al., 2018) provide a comprehensive review of thiophene PAHs, specifically as organic semiconductors, addressing current challenges, proposing future research directions, and aiming to inspire innovative applications semiconductor technology. (Das, Bhauriyal, & Pathak, 2020) elucidate that the flexible configuration of PAH molecules is expected to offset slightly elevated diffusion energy barrier values, particularly in the context of their potential application as cathodes in Aluminum Dual Ion Batteries (Al-DIBs). These findings encourage further exploration of PAH materials and analogous organic compounds specifically for their electronic application in battery technologies.

Employing advanced computational methods, specifically Density Functional Theory (DFT), allows for a thorough exploration of the electronic landscape, providing insights beyond the limitations imposed by experimental constraints. In a study conducted by (Kuamit, Ratanasak, Rungnim, & Parasuk, 2017), an investigation into the effects of size, shape, and pyrene doping on the electronic properties of graphene nanoflakes (GNFs) was undertaken. This study delved into two shapes of zigzag GNFs, hexagonal (HGN) and rhomboidal (RGN), shedding light on the correlation between the energy band gap of GNFs, their shape, and the subsequent decrease in size. Moreover, the introduction of pyrene and pyrene derivatives on both HGN and RGN offered valuable insights into the shifts in HOMO and LUMO energies, providing a nuanced perspective on the electronic properties of these nanoflakes.

In a distinct exploration, (Ramya & Suresh, 2023) utilized DFT calculations to investigate the electron distribution in PAHs as anode materials in Lithium-Ion Batteries. Building on this research, (Rakhi & Suresh, 2020), employing DFT calculations, reported a significant influence of the size and shape of PAHs on their optoelectronic properties, showcasing their potential applications in solar energy harvesting.

Taking the study of PAHs a step further, we focus specifically on Kekuléan PAHs, characterized by a unique structural motif inspired by the work of Friedrich August Kekulé. This subset introduces distinctive arrangements of fused benzene rings,

providing a platform for an in-depth investigation into how the Kekuléan structural motif influences the properties of PAHs. electronic Through DFT calculations, our study aims to unravel the intricate relationship between molecular architecture, particularly the Kekuléan motif, and electronic characteristics, contributing to a broader understanding of these captivating carbon-based materials.

EXPERIMENTAL SECTION Computational Details

Geometry optimizations were performed at the Kohn-Sham DFT level using Becke's three-parameter exchange with Lee-Yang-Parr correlation (B3LYP) in combination with the LANL2DZ basis set, which is already known as one of the best methods to study organic compound (Abkari et al., 2016; Aziz , Santoso, Mulya, & Pranowo, 2017; Fadjar Mulya, et al., 2016; Tounsi et al, 2016). The calculations were performed using the Gaussian 09 software package (Frisch et al., 2009). The PAHs were optimized for four Kekuléan geometries: Hexagonal, Linear, Rhombus, and Zigzag, chosen to represent stable Kekuléan configurations (see **Table 1**). To assess the robustness of the structural results with respect to the exchangecorrelation functional, the optimized geometries were subsequently re-optimized with three alternative hybrid functionals: HSEHPBE1, wB97XD, and PBEPBE, while preserving the same basis set and gas-phase conditions. All optimizations and subsequent analyses were performed in Gaussian09. Frequency analyses were conducted at the same level of theory to confirm that each optimized structure corresponds to a true minimum (no imaginary frequencies). The dispersioncorrected functional wB97XD was included to account for long-range interactions, while HSEHPBE1 and provide **PBEPBE** screened/exchange-correlation variants to test sensitivity to exchange treatment. Bond lengths, bond angles, and band gap energies Eg (and densities of states, DOS) were computed for each geometry and functional; a direct comparison across functionals is presented in **Table 2**, and the Eg values are summarized in Table 3. The LANL2DZ basis set was used consistently for all atoms. The DOS calculation was performed using GaussSum 2.0 package software.

Table 1. Geometry, size and notation used in this study

Geometry	Notation	Formula	Number of Rings (N)	
Hexagonal	H _n	$C_{6n^2}H_{6n}$	2n²-n	
Linear	L_n	$C_{4n+6}H_{6n+4}$	n+1	
Rhombus	R_n	$C_{6n^2}H_{6n}$	$(n+1)^2$	
Zigzag	Z_n	$C_{4n+10}H_{6n+10}$	n+2	

Proof: For an arbitrary PAHs, there are many ways to add a ring into the structure. But in practice, all of them can be classified into 5 positions depending on the number of adjacent rings.

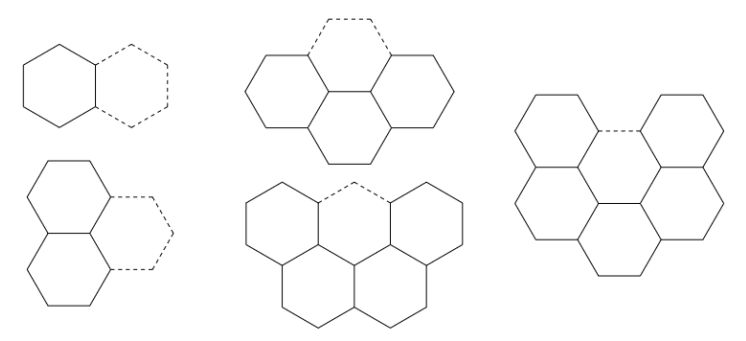


Figure 1. The 5 possible types of position for ring addition

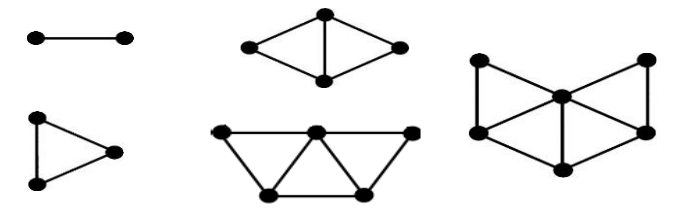


Figure 2. Graph representation of Figure 1.

In **Figure 1**, five possible positions for ring addition to an existing Kekuléan structure are illustrated. Since the previous structure is already Kekuléan, the addition of a ring while maintaining the Kekuléan structure can only occur if there is an even number of atoms added. Therefore, the ring can only be added to a position with an odd number of adjacent rings. By transforming all the rings into vertices and all the fused bonds into perpendicular edges connecting the vertices, the structures shown in **Figure 1** can be represented as graphs.

Figure 2 demonstrates that adding a new ring (vertices) to a Kekuléan structure will always result in two faces (triangles) with opposite orientations. It can be deduced that in a hexagonal representation of a PAH transformed into a graph, the number of faces is even and occurs in pairs if and only if the structure is Kekuléan.

Among the selected geometries, it is evident that Z_n and L_n are Kekuléan because they do not form any faces. R_n can always be constructed by two triangles with opposite orientations, making it Kekuléan. Hn is also Kekuléan as it can be constructed from three R structures in different orientations. This completes the proof that all selected geometries are Kekuléan.

RESULTS AND DISCUSSIONS Validation Methods

The realm of computational chemistry demands precise method selection, a critical step in establishing a reliable correlation with experimental outcomes. In the context of this investigation, the methodological approach embraced DFT calculations coupled with LANL2DZ basis functions and an array of hybrid functionals. The meticulous process of method selection unfolded through a comprehensive

comparison of computational results against empirical data, meticulously documented in **Table 2** and visually represented in **Figure 3** These comparisons specifically focused on the anthracene molecular system, scrutinizing parameters such as bond lengths and angles, thereby providing a robust foundation for the subsequent analytical insights.

Table 2 indicates that all utilized hybrid functionals yield optimized structures close to the crystallographic results (Cruickshank & Sparks, 1960). The relative average deviations for bond lengths from experiments are 0.4423%, 0.332%, 0.346%, and 0.748% for wB97XD, B3LYP, HSEHPBE1, and PBEPBE, respectively. Similarly, the average angular deviations for B3LYP, HSEHPBE1, wB97XD, and PBEPBE are 0.467%, 0.443%, 0.380%, and 0.468%, respectively. The average deviations below 1% demonstrate the accuracy of the employed hybrid functionals in predicting molecular structures. Nevertheless, the small differences in the calculated results are not significant enough to determine the best-performing hybrid functional.

To address this, additional parameters, such as the band gap value (Eg), were considered. (Sano, et al., 1965) measured the Eg value of anthracene using delayed electroluminescence, reporting Eg > 3.10 eV. (Vaubel & Baessler, 1968) employed photoemission methods and reported Eg $= 3.72 \pm 0.02$ eV. **Table 3** presents the calculated Eg values compared to experimental results. It is observed that the relative deviations for the B3LYP, HSEHPBE1, wB97XD, and PBEPBE hybrid functionals are 2.42%, 13.72%, 92.47%, and 35.75%, respectively, compared to measurements by Vaubel and Baessler. Based on these results, subsequent calculations will be conducted using the DFT/B3LYP/LANL2DZ method.

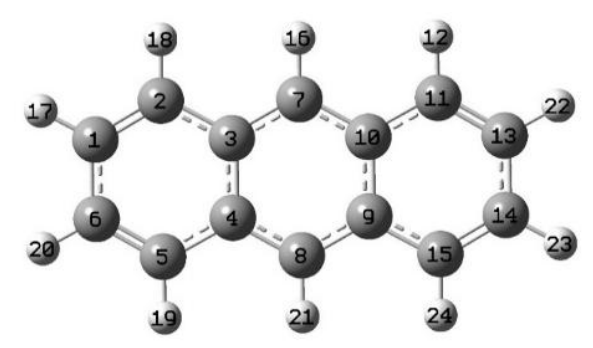


Figure 3. The numbering in the model of the molecular structure of anthracene

Table 2. Comparison of bond lengths and angles between computational results and experimental values.

Paramete	r	XRC ¹	B3LYP	HSEHPBE1	wB97XD	PBEPBE
Taramele						
Bond	2-1-6	120.783	120.433	120.418	120.477	120.422
	1-2-3	120.217	121.023	120.987	120.926	121.003
	2-3-4	119.000	118.544	118.595	118.627	118.574
angle (°)	7-3-4	119.517	119.069	119.099	119.191	119.048
	3-7-10	120.933	121.826	121.802	121.618	121.905
	1-2	1.368	1.371	1.368	1.363	1.380
Bond	1-6	1.419	1.428	1.423	1.429	1.430
length	2-3	1.436	1.432	1.427	1.433	1.434
(Å)	3-7	1.399	1.402	1.398	1.397	1.408
	3-4	1.428	1.447	1.442	1.437	1.455

¹Cruickshank dan Spark (1960)

Table 3. Comparison of calculated and measured Eg values.

Eg (eV)	
> 3.10	
3.72 ± 0.02	
3.63	
3.23	
7.16	
2.39	

¹Sano dkk. (1956)

Energy Profile

The energy of a system serves as a critical metric, providing insights into its overall stability. Within the domain of computational chemistry, the energy of a molecular system becomes a pivotal determinant, serving as a foundation from which all other molecular properties can be deduced. In the comprehensive analysis presented in **Table S1** and **Figure 4**, we delve into the intricate relationship between the molecular energy values of PAHs and their correlation with the size and shape of these molecules.

Table S1 and **Figure 4** collectively unravel the multifaceted interplay between the molecular energy of PAHs and the dimensions and configurations of the molecules. A discernible pattern emerges, indicating that the molecular energy of PAHs is inherently linked to their size. **Figure 4(a)** visually articulates this correlation, emphasizing that the molecular energy is

directly proportional to the number of rings in PAHs with linear geometry. This relationship is succinctly expressed by the equation:

$$E_L = -403350,471N - 206451,42$$
 (Eq.1)

Here E_L represents the molecular energy, and N is the number of rings. This phenomenon also occurs in PAHs with other geometries.

$$E_Z = -403329,095N - 206350,453$$
 (Eq.2)

$$E_H = -238607,162N - 666700,120$$
 (Eq.3)

$$E_R = -248398,691N - 749306,341$$
 (Eq.4)

 E_Z , E_H and E_R are, respectively, the energies for molecules with zigzag, hexagonal, and rhombic geometries. This quantitative representation unveils a compelling insight into the size-dependent nature of molecular energy within PAHs, revealing a profound connection between their structural characteristics and the associated energy values.

²Vaubel dan Baessler (1968)

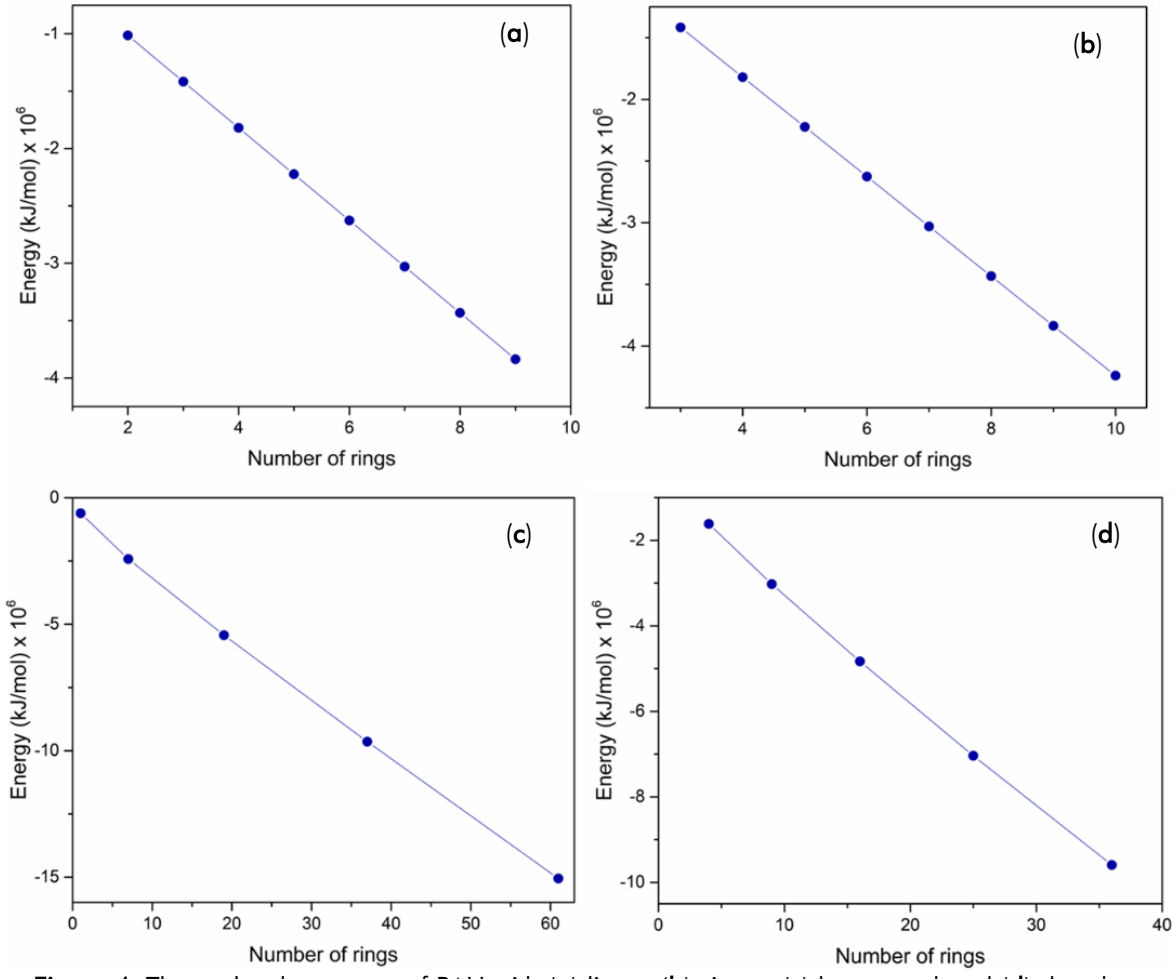


Figure 4. The molecular energy of PAH with (a) linear (b) zigzag (c) hexagonal and (d) rhombus

The equations above indicate that PAH with zigzag and linear geometries have lower energy compared to hexagonal and rhombic geometries. This is because PAH with linear and zigzag geometries have a higher number of atoms due to molecular growth, resulting in a relatively lower molecular energy compared to PAH with hexagonal and rhombic geometries.

Electronic Structure

 E_{HOMO} denotes the energy of the highest occupied molecular orbital and E_{LUMO} denotes the energy of the lowest unoccupied molecular orbital. By definition, the HOMO–LUMO gap is $Eg=E_{\text{LUMO}}-E_{\text{HOMO}}$. Our calculations show that the band gap energy Eg decreases as the number of rings N increases, with a geometry-dependent rate. Linear geometries (L_n) exhibit the strongest size dependence, followed by Rhombus (R_n) and Hexagonal (H_n) geometries. Zigzag (Z_n) geometries display confinement-like behavior, with Eg potentially plateauing at larger sizes. These trends are consistent with the general expectation that increased conjugation reduces the gap, while geometry modulates the rate of this reduction.

The density of states DOS, which quantifies the distribution of energy levels, shows a size-normalized behavior that is largely insensitive to N across all four

geometries L_n Z_n H_n R_n . While Eg decreases with increasing N, the DOS remains comparatively stable, reflecting its reduced sensitivity to size in these systems (Whitcher et al., 2016; Yang, Bussolotti, Kera, & Ueno, 2017). Geometric symmetry introduces characteristic differences in DOS values: L_n , Z_n , and R_n differ in their absolute DOS, and the high-symmetry Hn family tends to exhibit distinct DOS features. **Table S1** summarizes the computed DOS for the four geometries, and occasional near degeneracies (for example in certain Z_n states) can produce small fluctuations near the LUMO

Together, these results indicate that PAH size and geometry jointly tune electronic structure, with Eg showing a clear size- and geometry-dependent trend, while DOS behaves as a robust descriptor with geometry-imposed variations. Our qualitative trends align with broader observations in conjugated carbon systems: size drives a reduction in the band gap, and molecular geometry modulates the rate and manner of this reduction. The DOS's relative insensitivity to size supports its use as a stable comparative metric across geometries. These findings establish a basis for engineering Kekuléan PAHs for electronic and energy-storage applications and provide a concise point of contact with prior studies in the literature.

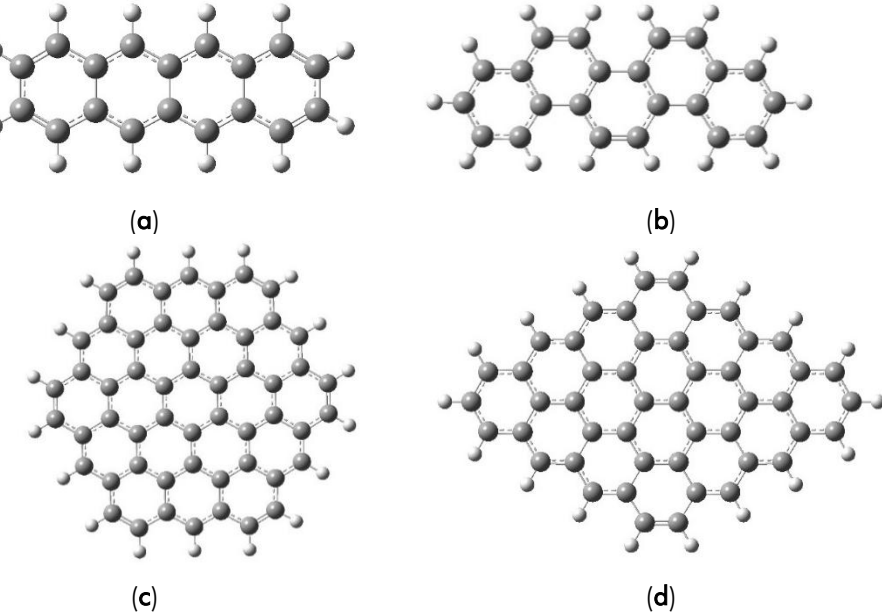


Figure 5. Optimized structure of (a) L_n , (b) Z_n , (c) H_n and (d) R_n

Linear and Zigzag

The presented calculation results showcase the frontier orbital energy and DOS spectra of L_n and Z_n , as illustrated in **Figure 6** and **Figure 7**. A notable observation from the figure is the gradual narrowing of the frontier orbital energy for both L_n and Z_n , as parameter N increases. This phenomenon contributes to a concurrent reduction in the energy gap (Eg) for both types of PAHs. Specifically, upon closer examination in **Figure 6c**, it becomes evident that $Eg^L(N)$ experiences a more rapid decrease compared to $Eg^Z(N)$.

The reduction in the energy gap as N increases indicates a size-dependent trend in the electronic structure of these PAHs. This observation may be attributed to the intricate interplay between molecular size and electronic properties. The differing rates of decrease between Eg^L(N) and Eg^Z(N) suggest nuanced variations in the electronic behaviors of linear and zigzag PAHs, emphasizing the importance of molecular geometry in influencing their electronic characteristics. The difference in the rate of decrease between Eg^L(N) and Eg^L(N) is due to the difference in their edge states, as shown in a previous study (X. Wang et al., 2008); (Mohanty et al., 2012), which also demonstrated that Eg^Z(N) > 0 for all N due to edge states and confinement.

Performing a straightforward numerical analysis on $Eg^Z(N)$ reveals that it is not strictly a decreasing function of N. This deviation from a strictly decreasing trend is attributed to the symmetry differences present in Z_n for even and odd values of N. The intricate relationship between molecular size and the symmetry of zigzag PAHs contributes to the observed variations in the energy gap with increasing N. In contrast, a parallel analysis on $Eg^L(N)$

demonstrates a clear and consistent pattern. $Eg^L(N)$ is determined to be a strictly decreasing function, indicating a more straightforward relationship between the energy gap and the linear PAH size. This distinction further underscores the importance of molecular geometry and symmetry considerations in comprehending the electronic characteristics of different PAH structures.

Extrapolation from the available values of $Eg^L(N)$ will indicate that $In(N) = o(Eg^L(N))$, where o(f(N)) is the little-o notation, signifying that $Eg^L(N)$ decreases faster than the growth of the logarithmic function. thus $Eg^L(N)$ would reach 0 eV for finite N.

Hexagonal and Rhombus

The results of the frontier orbital energy calculations and DOS spectra for H_n and R_n are graphically depicted in **Figure 8** and **Figure 9**. Notably, the electronic structure of H_n and R_n closely mirrors that of Ln. This resemblance is characterized by the shared trend of a strictly decreasing energy gap $Eg^R(N)$ and $Eg^H(N)$, as well as their asymptotic behavior when extrapolated from the available data. By subjecting this dataset to the same numerical analysis, it becomes apparent that the energy gap (Eg(N)) for these PAHs would also converge to 0 eV for finite N.

However, distinct differences emerge in the rates of decrease among L_n , R_n and H_n , with L_n exhibiting the fastest decrease, followed by R_n and H_n . This variation in the rate of decrease is attributed to the differing ratios of the number of edge states to the surface states, which can be approximated as the perimeter-to-area ratio. L_n , having no surface state, experiences the most rapid reduction in $Eg^L(N)$, while $Eg^H(N)$ undergoes the slowest decrease due to its high symmetry.

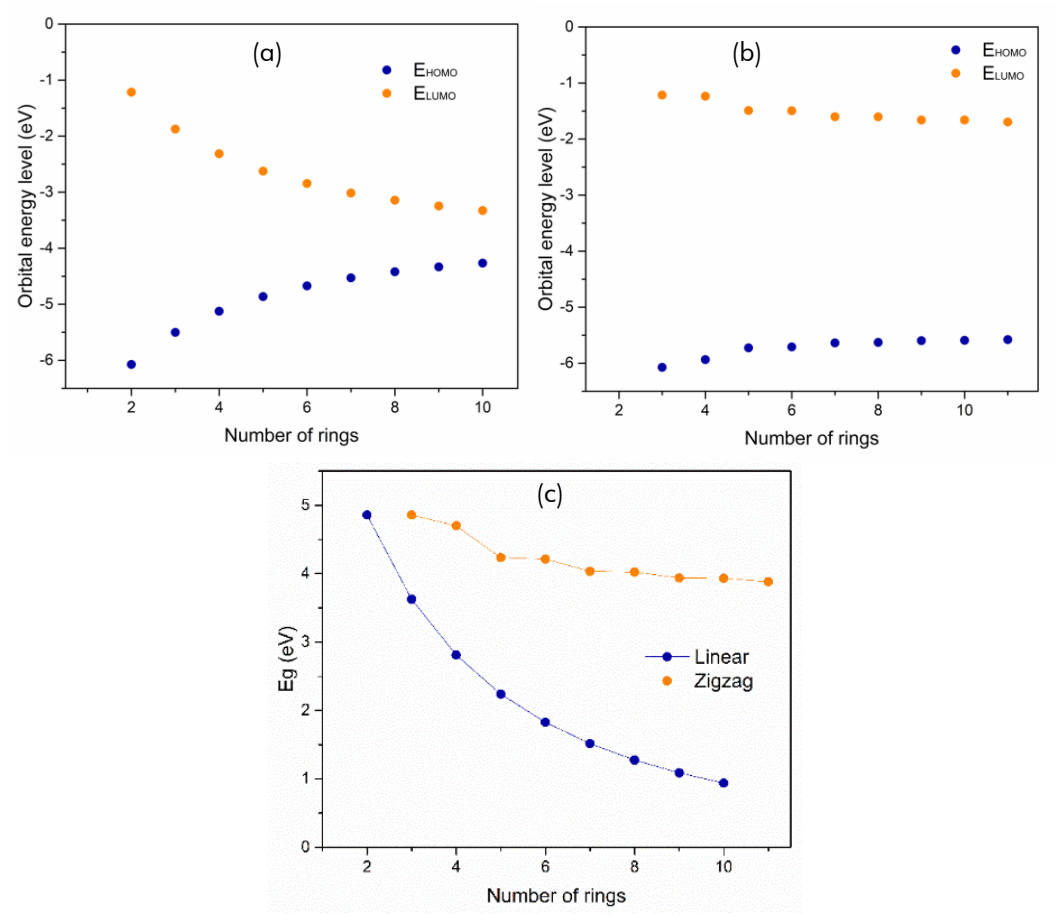


Figure 6. (a) Frontier Orbitals Energy of L_n , (b) Frontier Orbitals Energy of Z_n , (c) Comparison Eg(N) between L_n and Z_n

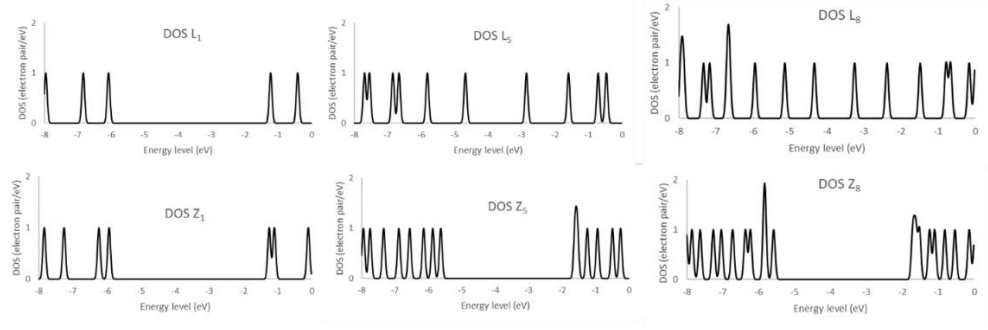
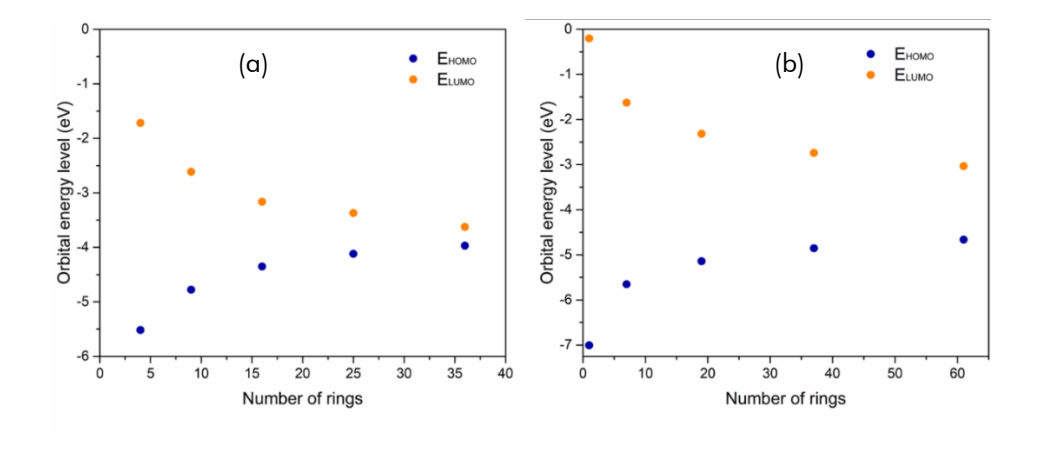


Figure 7. DOS spectra L_1 , L_5 , L_8 , Z_1 , Z_5 and Z_8



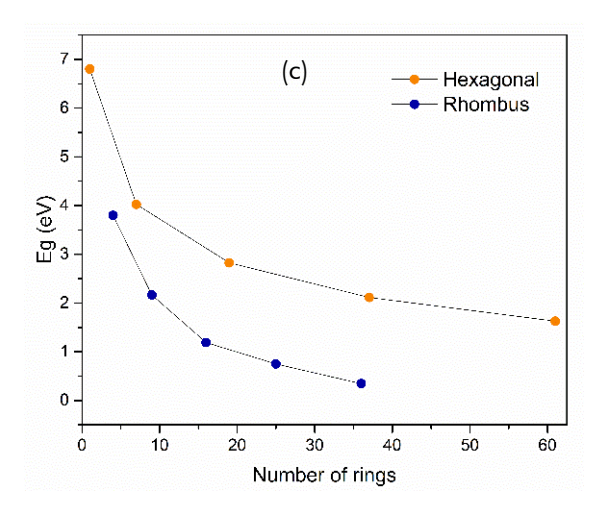


Figure 8. (a) Frontier Orbitals Energy of R_n , (b) Frontier Orbitals Energy of H_n , (c) Comparison Eg(N) between R_n and H_n

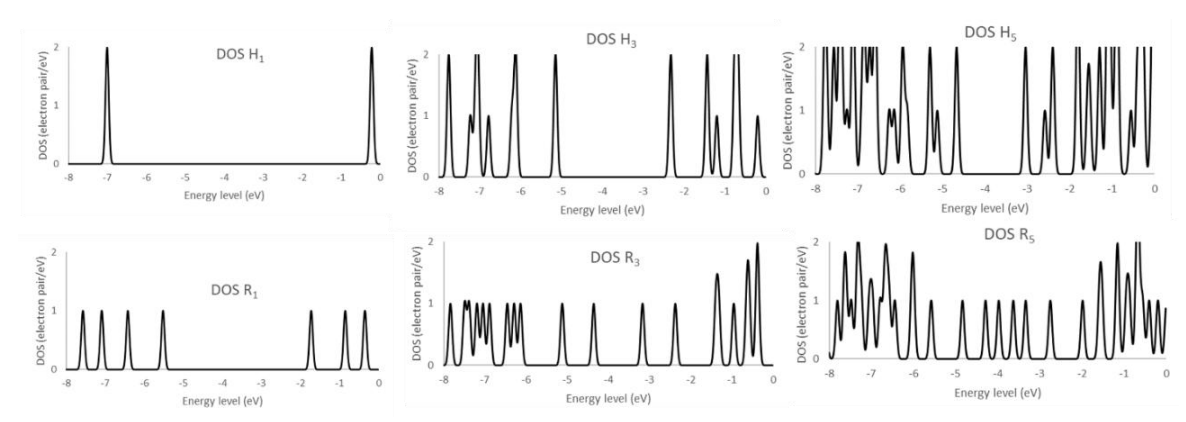


Figure 9. DOS spectra H_1 , H_3 , H_5 , R_1 . R_3 , and R_5

This intricate analysis not only highlights the commonalities in the electronic structure trends among these PAHs but also unveils the underlying factors contributing to the observed variations in their respective energy gap behaviors. The nuanced interplay between the molecular geometry, surface states, and symmetry characteristics adds depth to our understanding of the electronic properties exhibited by these diverse PAH structures.

CONCLUSIONS

In summary, our DFT-based investigation into Kekuléan Polycyclic Aromatic Hydrocarbons (PAHs) reveals a consistent decrease in band gap energy as the number of rings increases. Molecular size plays a crucial role, with linear PAHs showing the fastest reduction, followed by rhombic and hexagonal PAHs, while zigzag PAHs exhibit confinement-related behavior where Eg may plateau. Notably, the decrease in Eg outpaces the growth of the logarithmic term, suggesting Eg tends toward zero at finite size. This study further shows that PAH size affects Eg but not the DOS, and that molecular geometry modulates both Eg and DOS, with the lowest Eg values for linear, rhombic, hexagonal, and zigzag geometries in that order. Based on these trends, we provide actionable

recommendations: tailor PAH size and geometry to optimize Eg for LIB anodes to balance energy density and rate capability; synthesize representative Linear, Zigzag, Hexagonal, and Rhombus PAHs and perform comprehensive electrochemical testing to validate the predicted trends and assess cycling stability; incorporate PAHs into conductive composite electrode formulations to enhance electronic percolation and mechanical integrity, enabling scalable and durable electrode architectures; pursue scalable, cost-effective synthesis and processing routes for the target geometries and sizes; and extend the computational model to include solvent and electrolyte effects and intercalation energetics to better translate these materials to real battery environments. These recommendations aim to translate Kekuléan PAHs from fundamental understanding to practical applications in LIB technology and related domains.

ACKNOWLEDGEMENTS

Authors are grateful to Austrian-Indonesian Centre for Computational Chemistry, Universitas Gadjah Mada, for the computer time and facilities. Authors would also like to acknowledge the contribution from our late mentor, Dr. Ria Armunanto for his insights and supervision during this study.

REFERENCES

- Abkari, A., Chaabane, I., & Guidara, K. (2016). DFT (B3LYP/LanL2DZ and B3LYP/6311G+ (d, p)) comparative vibrational spectroscopic analysis of organic–inorganic compound bis (4-acetylanilinium) tetrachlorocuprate (II). Physica E: Low-dimensional Systems and Nanostructures, 81, 136-144.
- Alden Mostaan, S. M., & Saghaei, H. (2021). A tunable broadband graphene-based metamaterial absorber in the far-infrared region. *Optical and Quantum Electronics*, 53(2), 96.
- Aumaitre, C., & Morin, J. F. (2019). Polycyclic aromatic hydrocarbons as potential building blocks for organic solar cells. *The Chemical Record*, 19(6), 1142-1154.
- Aziz, H. A., Santoso, G. A., Mulya, F., & Pranowo, H. D. (2017). Molecular and electronic structure of some symmetrically meso-substituted Hg (II)-porphyrin complexes. *Asian Journal of Chemistry*, 29(10), 2224-2226.
- Cruickshank, D. W. J., & Sparks, R. A. (1960). Experimental and theoretical determinations of bond lengths in naphthalene, anthracene and other hydrocarbons. *Proceedings of the Royal Society of London. Series A. Mathematical and Physical Sciences*, 258(1293), 270-285.
- Das, S., Bhauriyal, P., & Pathak, B. (2020). Polycyclic aromatic hydrocarbons as prospective cathodes for aluminum organic batteries. *The Journal of Physical Chemistry C*, 125(1), 49-57.
- Fakih, I., Durnan, O., Mahvash, F., Napal, I., Centeno, A., Zurutuza, A., . . . Szkopek, T. (2020). Selective ion sensing with high resolution large area graphene field effect transistor arrays. *Nature communications*, 11(1), 3226.
- Frisch, M. J., Trucks, G. W., Schlegel, H. B., Scuseria, G. E., Robb, M., Cheeseman, J. R., Petersson, G. A. (2009). Gaussian Inc. Wallingford Ct, 2009.
- Guo, L., Zhang, Q., & Chan, K. S. (2021). A dual-gate field-effect transistor in graphene heterojunctions. *Superlattices and Microstructures, 150,* 106778.
- Jiang, L., Yuan, C., Li, Z., Su, J., Yi, Z., Yao, W., . . . Pan, M. (2021). Multi-band and high-sensitivity perfect absorber based on monolayer graphene metamaterial. *Diamond and Related Materials*, 111, 108227.
- Katsnelson, M. I. (2020). *The Physics of graphene* (2 ed.). Cambridge: Cambridge University Press.
- Kim, T., Fan, S., Lee, S., Joo, M.-K., & Lee, Y. H. (2020). High-mobility junction field-effect transistor via graphene/MoS2 heterointerface. *Scientific reports, 10*(1), 13101.
- Kuamit, T., Ratanasak, M., Rungnim, C., & Parasuk, V. (2017). Effects of shape, size, and pyrene

- doping on electronic properties of graphene nanoflakes. *Journal of molecular modeling, 23,* 1-9.
- Kumar, R., Sahoo, S., Joanni, E., Singh, R. K., Maegawa, K., Tan, W. K., . . . Matsuda, A. (2020). Heteroatom doped graphene engineering for energy storage and conversion. *Materials Today, 39*, 47-65.
- Larik, F. A., Faisal, M., Saeed, A., Abbas, Q., Kazi, M. A., Abbas, N., Channar, P. A. (2018). Thiophene-based molecular and polymeric semiconductors for organic field effect transistors and organic thin film transistors. *Journal of Materials Science: Materials in Electronics, 29*, 17975-18010.
- Lin, K.-T., Lin, H., Yang, T., & Jia, B. (2020). Structured graphene metamaterial selective absorbers for high efficiency and omnidirectional solar thermal energy conversion. *Nature communications*, 11(1), 1389.
- Mohanty, N., Moore, D., Xu, Z., Sreeprasad, T. S., Nagaraja, A., Rodriguez, A. A., & Berry, V. (2012). Nanotomy-based production of transferable and dispersible graphene nanostructures of controlled shape and size. *Nature communications*, 3(1), 844.
- Mulya, F., & Parasuk, V. (2020). Tetrachloroaluminate ion on graphene quantum dots: Towards the design of cathode for aluminum-ion battery.
- Mulya, F., Santoso, G. A., Aziz, H. A., & Pranowo, H. D. (2016). Design a better metalloporphyrin semiconductor: A theoretical studies on the effect of substituents and central ions.
- Muthuvinayagam, M., Ashok Kumar, S. S., Ramesh, K., & Ramesh, S. (2023). Introduction of graphene: The "Mother" of all carbon allotropes *graphene: fabrication, Properties* and Applications (pp. 5-20): Springer.
- Naumis, G. G., Barraza-Lopez, S., Oliva-Leyva, M., & Terrones, H. (2017). Electronic and optical properties of strained graphene and other strained 2D materials: a review. *Reports on Progress in Physics*, 80(9), 096501.
- Papageorgiou, D. G., Kinloch, I. A., & Young, R. J. (2017). Mechanical properties of graphene and graphene-based nanocomposites. *Progress in materials science*, *90*, 75-127.
- Qi, Y., Zhang, Y., Liu, C., Zhang, T., Zhang, B., Wang, L., . . . Wang, X. (2020). A tunable terahertz metamaterial absorber composed of elliptical ring graphene arrays with refractive index sensing application. Results in Physics, 16, 103012.
- Rahayu, E. F., Bunnari, B., & Hardyansyah, A. (2020). Reduction of Graphene Oxide: Controlled Synthesis by Microwave Irradiation. *Molekul*, 15(1), 56-62.
- Rakhi, R., & Suresh, C. H. (2020). Optoelectronic properties of polycyclic aromatic hydrocarbons

- of various sizes and shapes: a DFT study. *Beilstein Archives, 2020*(1), 119.
- Ramya, P. K., & Suresh, C. H. (2023). Polycyclic aromatic hydrocarbons as anode materials in lithium-ion batteries: a dft study. *The Journal of Physical Chemistry A*, 127(11), 2511-2522.
- Rozhkov, A. V., Sboychakov, A. O., Rakhmanov, A. L., & Nori, F. (2016). Electronic properties of graphene-based bilayer systems. *Physics Reports*, 648, 1-104.
- Saito, R., Dresselhaus, G., Dresselhaus, M. S., Dresselhaus, G., & Dresselhaus, M. S. (1998). *Physical properties of carbon nanotubes* (Vol. 203): Imperial college press London.
- Sano, M., Pope, M., & Kallmann, H. (1965). Electroluminescence and band gap in anthracene. *The Journal of Chemical Physics*, 43(8), 2920-2921.
- Tounsi, A., Hamdi, B., Zouari, R., & Salah, A. B. (2016). DFT (B3LYP/LanL2DZ), non-linear optical and electrical studies of a new hybrid compound:[C6H10 (NH3) 2] CoCl4· H2O. *Physica E: Low-dimensional Systems and Nanostructures, 84*, 384-394.
- Tyutyulkov, N., Madjarova, G., Dietz, F., & Müllen, K. (1998). Is 2-D graphite an ultimate large hydrocarbon? 1. Energy spectra of giant polycyclic aromatic hydrocarbons. *The Journal of Physical Chemistry B, 102*(50), 10183-10189.

- Vaubel, G., & Baessler, H. (1968). Determination of the band-gap in anthracene. *Physics Letters A*, 27(6), 328-329.
- Wang, A., Zhao, C., Yu, M., & Wang, W. (2021). Trifunctional Co nanoparticle confined in defect-rich nitrogen-doped graphene for rechargeable Zn-air battery with a long lifetime. *Applied Catalysis B: Environmental, 281*, 119514.
- Wang, X., Ouyang, Y., Li, X., Wang, H., Guo, J., & Dai, H. (2008). Room-temperature all-semiconducting sub-10-nm graphene nanoribbon field-effect transistors. *Physical review letters*, 100(20), 206803.
- Wen, J., Yan, C., & Sun, Z. (2020). The application of a high-κ polymer dielectric in graphene transistors. *Advanced Electronic Materials*, *6*(7), 2000031.
- Whitcher, T. J., Wong, W. S., Talik, A. N., Woon, K. L., Chanlek, N., Nakajima, H., . . . Songsiriritthigul, P. (2016). Investigation into the Gaussian density of states widths of organic semiconductors. *Journal of Physics D: Applied Physics*, 49(32), 325106.
- Yang, J.-P., Bussolotti, F., Kera, S., & Ueno, N. (2017). Origin and role of gap states in organic semiconductor studied by UPS: as the nature of organic molecular crystals. *Journal of Physics D: Applied Physics, 50*(42), 423002.